Impact of measured and simulated tundra snowpack properties on heat transfer

Victoria R. Dutch[1], Nick Rutter[1], Leanne Wake[1], Melody Sandells[1], Chris Derksen[2], Branden Walker[3], Gabriel Hould Gosselin[4], Oliver Sonnentag[4], Richard Essery[5], Richard Kelly[6], Phillip Marsh[3], Joshua King[2]

[1] Department of Geography and Environmental Sciences, Northumbria University, Newcastle upon Tyne, UK
[2] Climate Research Division, Environment and Climate Change Canada, Toronto, Canada
[3] Cold Regions Research Centre, Wilfrid Laurier University, Waterloo, Canada
[4] Département de géographie, Université de Montréal, Canada
[5] School of Geosciences, University of Edinburgh, UK
[6] Department of Geography and Environmental Management, University of Waterloo, Canada

Correspondence to: Victoria Dutch (victoria.dutch@northumbria.ac.uk)

Abstract.

Snowpack microstructure controls the transfer of heat to, and the temperature of, the underlying soils. In situ measurements of snow and soil properties from four field campaigns during two different winters (March and November 2018, January and March 2019) were compared to an ensemble of CLM5.0 (Community Land Model) simulations, at Trail Valley Creek, Northwest Territories, Canada. Snow MicroPenetrometer profiles allowed snowpack density and thermal conductivity to be derived at higher vertical resolution (1.25 mm) and a larger sample size (n = 1050) compared to traditional snowpit observations (3 cm vertical resolution; n = 115). Comparing measurements with simulations shows CLM overestimated snow thermal conductivity by a factor of 3, leading to a cold bias in wintertime soil temperatures (RMSE = 5.8 °C). Bias-correction of the simulated thermal conductivity (relative to field measurements) improved simulated soil temperatures (RMSE = 2.1 °C). Multiple linear regression shows the required correction factor is strongly related to snow depth (R^2 = 0.77, RMSE = 0.066) particularly early in the winter. Furthermore, CLM simulations did not adequately represent the observed high proportions of depth hoar. Addressing uncertainty in simulated snow properties and the corresponding heat flux is important, as wintertime soil temperatures act as a control on subnivean soil respiration, and hence impact Arctic winter carbon fluxes and budgets.

1 Introduction

Seasonal snow is an effective insulator, with snow thermal properties influencing the soil microclimate (Lawrence and Slater, 2009; Wilson et al., 2020) and the distribution and state of permafrost (Biskaborn et al., 2019; Goncharova et al., 2019; Zhang, 2005). The temperature of the subnivean environment, particularly the extent to which it allows for the presence of small amounts of liquid water, acts as an important control on biogeochemical cycling, including soil respiration (Semenchuk et al., 2015; Sullivan et al., 2008; Williams et al., 2009). In addition, the soil temperature also impacts the hydrology through controls on soil infiltration and runoff (Niu and Yang, 2006; Quinton and Marsh, 1999). Accounting for how well the thermal and hydrological conditions of subnivean soils (including the physical state of soil water content) are simulated is therefore critical for understanding how well current land models such as the Community Land Model (CLM; Lawrence et al. (2019)) can be expected to simulate winter carbon fluxes (e.g. Natali et al. (2019)) and permafrost evolution (Koven et al., 2012).

The depth, [micro]structure, and stratigraphy of the snowpack determine its capacity to insulate the underlying soil and are in turn influenced by the temperature of the ground surface. Tundra snowpacks typically consist of a basal depth hoar layer, formed as strong temperature gradients within the snowpack induce kinetic metamorphism, overlain by an upper wind slab layer, compacted and densified over the course of a snow season by strong Arctic winds (Sturm et al. (1995), Derksen et al, (2009; 2014); Rees et al. (2014), among others). Between these two layers, an indurated hoar layer may also be formed, where

the lower part of the wind slab takes on some of the microstructural properties of depth hoar while maintaining the density and hardness of a wind slab (Derksen et al., 2009).

45 The thermal influence of the snowpack on the underlying soil can be considered in terms of an effective snow depth ($S_{depth,eff}$), which describes the insulative properties of the snowpack by weighting the mean monthly snow depth by its relative position in the season at a given location across an entire winter (October – March) (Slater et al., 2017); emphasizing the timing of snow accumulation as more important than the end of season snow depth in determining wintertime soil temperatures (Lafrenière et al., 2013). Rapid snow accumulation and snowpack establishment early in the winter will insulate the ground

50 thereby dampening soil temperature fluctuations, leading to a higher $S_{depth,eff}$ than steady accumulation throughout the entire winter, even if the total amount of precipitation is the same (Slater et al., 2017). The relationship between $S_{depth,eff}$ and the normalised temperature difference between air and soil (A_{norm}) can be used to understand heat transfer between the air and the soil and through the snowpack (Slater et al., 2017). The deviation of this relationship from the expected exponential form (Slater et al. (2017) - Fig. 3), termed the Snow Heat Transfer Metric (SHTM), can be calculated and used to evaluate simulated

55 heat transfer processes in the soil and snowpack as was undertaken by (Slater et al., 2017) for the land surface components of participating models in the CMIP5 model intercomparison project (Taylor et al., 2012). The closer the value of the SHTM is to one, the smaller the disagreement between modelled and observed air and soil temperature differences. Being able to quantitatively assess snow heat transfer is of particular importance because model parameterizations of snow physical properties can lead to differences in soil temperature and therefore contribute to uncertainties in estimates of Arctic winter

60 carbon fluxes and budgets, which are currently not well constrained (Fisher et al., 2014; Natali et al., 2019; Virkkala et al., 2021).

The effective thermal conductivity of the snowpack (K_{eff}; heat conducted through ice and interstitial air) determines the rate of heat transfer to underlying soil (Domine et al., 2015; Jafarov et al., 2014). From here on, we refer to the effective thermal conductivity of the snowpack as snow thermal conductivity for brevity, after Jafarov et al. (2014). Snow has a low thermal

65 conductivity, typically in the range 0.01 – 0.7 $Wm^{-2} K^{-1}$ (Gouttevin et al., 2018). Typical K_{eff} values for tundra snowpacks are at the lower end of this range, for example Domine et al. (2016) found a maximum value of 0.33 $Wm^{-2} K^{-1}$. Measurement of snow thermal conductivity is typically undertaken using a heated needle probe (Morin et al., 2010), although snow anisotropy causes 29 % uncertainty in these estimates of K_{eff} (Domine et al., 2015), which is a notable limitation to this method (Riche and Schneebeli, 2013). Models typically parameterise K_{eff} as a function of the simulated snow density (Gouttevin et al., 2018),

70 for which a number of different statistical relationships have been proposed (Sturm et al., 1997; Calonne et al., 2011).

This study characterises the variability of the thermal properties of tundra snow and resultant soil temperatures at Trail Valley Creek, Northwest Territories, Canada, over the 2017 - 18 and 2018 - 19 winters using in situ measurements. We then use these measurements to evaluate an ensemble of simulations from the Community Land Model (CLM5.0), particularly with regard to how thermal properties are simulated and the sensitivity of soil temperatures and SHTM to the properties of the snowpack.

2 Data and methods

2.1 Study location

Trail Valley Creek (TVC; 68°45'N, 133°30'W) is a 57 km^2 boreal: tundra transition research watershed located in the Inuvialuit Settlement Region, approximately 55 km northeast of Inuvik, NWT, Canada. TVC has an average elevation of approximately 99 m above sea level (Marsh et al., 2008) and a mean annual air temperature of -7.9 °C for the period 1999 - 2018 (Grünberg

80 et al., 2020). Land cover at TVC predominantly consists of graminoid tundra, with some lakes, small clusters of willow and alder shrubs and some isolated black spruce stands (Essery and Pomeroy, 2004; Grünberg et al., 2020; King et al., 2018). The terrain consists of mineral soil hummocks of up to a metre in diameter, and peaty inter-hummock hollows (Quinton and Marsh, 1998). The ground is underlain by continuous permafrost to a depth of 350 - 500 m (Wilcox et al., 2019), with a maximum

active layer depth of up to 1 m at the end of the summer (Grünberg et al., 2020). Snow cover at TVC has a typical duration of
85 8 months (Pomeroy et al., 1993), with typical depths of 0.2 - 0.5 m, though drifts of up to 2m occur surrounding tall shrubs
and in proximity to steep slopes (Marsh and Pomeroy, 1999).

2.2 Field methods

Comprehensive snow and soil data are used from four winter season intensive measurement periods (14 - 21 March 2018; 12
- 18 November 2018, 11 – 20 January 2019, and 18 – 27 March 2019). Additionally, meteorological data for the entirety of
90 the study period (1 August 2017 – 31 August 2019; plus model spin-up), measured at the TVC eddy covariance tower (AWS)
were also used. Half-hourly 2 m air temperatures were measured using a HMP35CF sensor (Campbell Scientific, Logan, Utah)
and precipitation totals were measured using a weighted T-200B gauge (Geonor Inc., Branchville, New Jersey). Precipitation
gauge under-catch is common in tundra environments such as TVC (Smith, 2008; Watson et al., 2008; Gray and Male, 1981),
therefore precipitation was corrected as per Pan et al. (2016). Automated snow depth measurements used were from the nearby
95 Meteorological Service of Canada station and measured a SR50a sensor (Campbell Scientific). Soil temperature profiles were
measured at 2, 5, 10 and 20 cm depths using 107B Thermistors (Campbell Scientific). Soil moisture content was profiled at
the same depths using CS615 soil water content reflectometers (Campbell Scientific).

Spatially distributed Snow MicroPenetrometer (SMP; (Schneebeli and Johnson, 1998) profiles (n = 1050) were measured
across the TVC sub-catchment. The SMP provides vertical profiles of force at 40 µm resolution (Proksch et al., 2015). Bespoke
100 coefficients for tundra snowpacks, based on the work of King et al. (2020b), were calculated to derive high vertical resolution
snow density profiles from the SMP force profiles (see Appendix A for detailed methodology). These profiles were then used
to approximate profiles of thermal conductivity using the K_{eff} relationships derived by Sturm et al. (1997) and Calonne et al.
(2011), denoted $K_{eff\text{-}Sturm}$ and $K_{eff\text{-}Calonne}$ respectively.

During the March 2018 and March 2019 campaigns, thermal conductivity was also measured using a TP02 needle probe
105 (Hukseflux, Delft, Netherlands) after Morin et al. (2010). Measurements of thermal conductivity of each snowpack layer, a
total of 105 measurements from 37 different snowpits, were made across these two campaigns. Almost 36,5000 GPS located
snow depths (Toose et al., 2020; King et al., 2020a) were measured across the 4 campaigns using a Magnaprobe instrument
(Sturm and Holmgren, 2018), allowing spatial distributions of snow depths across the catchment to be examined. Vertical
profiles of snow density, using a 100 cm³ box cutter (Conger and Mcclung, 2009), and snowpack temperature were measured
110 at all snowpit locations for each campaign. Stratigraphic information profiled in each snowpit (n = 115) was used to assign
layer types to the measured densities (Fierz et al., 2009). Four layers (surface snow, wind slab, indurated hoar and depth hoar)
were visually identified in order to assess spatial variability in the thickness and properties of different snowpack layers.

2.3 Snowpack simulations

The Community Land Model v5.0 (CLM; Lawrence et al. (2019) is the land surface component of the Community Earth
115 System Model v2.0, which can be run at a variety of spatial scales. In this study, 1D "point mode" (a 0.1° x 0.1° grid cell)
CLM (PTCLM) simulations were centred at the location of the TVC station. Minor adjustments were made to the model,
namely that the snow accumulation factor was increased (following Swenson and Lawrence, 2012), from 0.1 to 2, and the
standard deviation of elevation set to 0.5 m after Malle et al. (2021), in order to emulate point-scale processes. These
adjustments limit the period of fractional snow cover, so that PTCLM represents a binary state of snow presence or absence
120 over a flat surface.

PTCLM simulations were run from August 2017 to August 2019, with model spin-up from January 2013. Spin-up was
necessary in order to allow soil temperatures to equilibrate. Variation between model runs with the same parameterisation after
more than 2 full years of spin-up is limited to ~ 1 °C throughout the top 5 m of the soil column. The impact of spin-up on soil
temperature is further discussed in Appendix B.

125 Simulations were forced with gap-filled AWS data from TVC. Following Essery et al. (2016), gaps of 4 hours or less filled using linear interpolation and larger gaps filled using ERA5 reanalysis data (Hersbach et al., 2020). Daily precipitation amounts from the AWS were converted to the hourly resolution required by CLM using the fraction of daily precipitation at each hourly timestep from ERA5. ERA5 reanalysis data was also used to partition precipitation into rain and snow for comparison against the linear ramp used by CLM. All precipitation falling when air temperatures are below 0 °C is classed as snow, after which

130 point an increasing proportion of the precipitation is classed as rain until air temperatures are above 2 °C where all precipitation is classed as rain (Lawrence et al., 2019).

CLM produces a computationally-layered snowpack, with the number of snow layers dependant on the snowpack depth, up to a theoretical maximum of 12 layers. Once the total snow depth exceeds a given threshold, the initial snow layer is subdivided into two layers with equal properties. Snow layer formation continues in this manner as layer thicknesses surpass the prescribed

135 ranges given in Jordan (1991). When a layer divides, the new layer is formed beneath it, rather than new layers being formed at the surface by new snowfall. As this process is not stratigraphically representative, layers are not described by snow type (for example, as per Fierz et al. (2009)), but instead numbered from the snow surface down. Each layer is parameterised using layer thickness, temperature and mass of water and ice, as per Anderson (1976), Dai and Zeng (1997) and Jordan (1991). Snow depths below 1 cm are not discretely modelled and are instead combined into the surface soil layer.

140 Density, thickness and thermal conductivity are output as a daily mean for each layer. CLM calculates snow density as a function of the relative proportions of ice (mass of ice = m_i) and liquid water (mass of liquid water = m_{lw}), weighted by the snow cover fraction (F_{sno}) for each grid cell:

$$\rho = \frac{m_i + m_{lw}}{F_{sno} \times h_{sl}} \tag{1}$$

145 Model adjustments outlined above lead to a snow fraction of 1 when snow is present, and 0 when snow is absent, reducing potential errors in simulated snow layer densities. Liquid water in the snowpack is zero until the start of melt out, and so in practice the computed snow layer density simplifies to the mass of ice (m_i) divided by the height of the snow layer (h_{sl}). These computed snow layer densities are then used to calculate snow layer thermal conductivities (K_{eff}), as per Jordan (1991):

150 $$K_{eff} = K_{air} + \left(\left((7.75 \times 10^{-5} \times \rho) + (1.105 \times 10^{-6} \times \rho^2) \right) (K_{ice} - K_{air}) \right) \tag{2}$$

Values for K_{ice} and K_{air}, the effective thermal conductivities of ice and interstadial air, are given in Lawrence et al. (2018). CLM uses 25 soil layers of increasing thickness (down to a depth of 49 m) to simulate soil thermal processes and simulates the properties of these layers at an hourly resolution. Despite the simplicity of the snowpack scheme included in CLM, which

155 does not represent the development of depth hoar layers (Van Kampenhout et al., 2017), previous evaluation of snow heat transfer in CLM4.0 (Slater et al. (2017) suggests this modelling framework should perform well.

3 Results

3.1 Observed meteorological, and soil moisture and thermal conditions

Minimum air temperatures of -33.9 °C (2018) and -36.9 (2019) were reached in early January, with a maximum air temperature

160 of 19.4 °C reached on 23 July 2018 (Fig. 1a). Mean annual air temperature for 2017 - 2019 was -7.4 °C, with the growing season between the two winters of interest, herein defined as when mean daily air temperatures were consistently above freezing, lasting for 102 days (31 May – 22 September 2018). The cold period was twice as long as the growing season, with consistent subfreezing air temperatures from 10 October 2017 to 30 May 2018 (232 days) and from 23 September 2018 to 11 May 2019 (230 days).

165 The first snowfall in winter 2017 - 18 was on 29 September and on 1 September in winter 2018 - 19. Precipitation phase was mixed between rain and snow for the first two weeks of the snow season in both winters (Fig. 1b), preventing the onset of snow accumulation. Figure 1c shows snowpack initiation in 2018 - 19 was 26 days earlier than in the previous year, with snow-on dates of 25 September 2018 and 21 October 2017 respectively. Soil freeze-up began with the onset of snowfall (Fig. 1b and d); 5 cm soil temperatures dropped to 0 °C on 13 October in 2017 and a month earlier on 15 September in 2018. Soil

170 temperatures remained around 0 °C as the soil froze and released latent heat. Soil saturation increased with depth causing a slower rate of soil freeze-up. Alonger freeze-up in 2018 was evident from the more gradual liquid soil moisture decrease, particularly at depth (20 cm). Deeper soil (20 cm) stayed at 0 °C for longer than soil nearer the surface (5 cm), and generally remained warmer until the start of the thaw period.

Variations in soil temperature, in response to diurnal and synoptic weather patterns of energy inputs from the atmosphere,

175 became increasingly muted with depth in the soil column once the snowpack was established. Anomalously warm mid-winter air temperatures that approached 0 °C (22 December 2017 and 9 February 2019) or exceeded 0 °C (18 and 31 March 2019, with a rain-on-snow event occurring on the latter of these dates) had little influence on the soil temperature profile (Fig. 1d) as air and soil temperatures were decoupled due to snow insulation. A maximum snow depth of 51 cm (2017/18) and 59 cm (2018/19) was measured at the AWS on 14 April 2018 and 11 May 2019 respectively. Snow depth from spatially distributed

180 magnaprobe measurement showed a greater difference in snow depth between the two years; mean March snow depths were 11 cm higher in 2018 - 19 than 2017 – 18. Magnaprobe measurements also gave a higher mean March snow depth than the AWS, with March 2018 snow depths were more heavily skewed than snow depths in 2019 (Fig. 2a). Minimum soil temperatures at both 5 cm (-10.9 °C) and 20 cm (-10.1 °C) depths in winter 2017 – 18 were colder than the following year (-9.5 °C and -8.2 °C), when the combined effect of earlier snowpack initiation and a deeper snow cover prevented colder soil

185 temperatures being reached. Soil temperatures remained fairly constant until sharply increasing in early May, with the duration of soil thaw 36 and 44 days in spring 2018 and 2019 respectively. Snow-off date, as measured at the AWS snow depth sounder, was one week later in 2017 - 18 (30 May) than in the following year (23 May). Soil temperatures at 5 cm increased above 0 °C for the first time on the final day of the snowmelt period in both years (Fig. 1d), with a five (2017 - 18) to seven (2018 - 19) day lag in the 20 cm soil temperatures.

190 **3.2 Measured snow properties**

Median density profiles from the SMP fall within the interquartile range of measured densities from volumetric sampling in snowpits (Table 2). Snowpacks in all three campaigns (Fig. 2b-d) had a very thin surface snow layer (composed of recently deposited snowfall), with low near-surface snow densities (< 300 kg m^{-3}) rapidly increasing in the top 5 % of the snowpack. A higher density (~ 320 kg m^3) wind slab layer was evident between 5 - 30 % of normalised depth from the snow surface. The

195 next ~ 10 % of the profile was a transitional section where density decreased by about 100 kg m^3, with the lowest ~ 60 % dominated by a lower density (~ 230 kg m^3) depth hoar layer. Differences between median layer densities exceed the ~ 10 % sampling error associated with the use of density cutters (Proksch et al., 2016; Conger and Mcclung, 2009), and in all but one instance, there was no overlap in the interquartile ranges of different snow layers within a campaign (Fig. 3). Densities between 40 – 80 % of normalised depth are likely overestimated due to microstructural assumptions made by the algorithm of Proksch

200 et al. (2015), which prevent the calculation of SMP densities below 200 kg m^3 (see Appendix).

The transitional section, or indurated hoar layer, with transitioning properties between wind slab and depth hoar, evident at between ~ 30 – 40 % depth, is often difficult to capture through traditional snowpit density profiles due to the 3 cm vertical resolution of density cutters and the layer being more defined by its ice crystal shape than density alone. The SMP enabled the detection of such features due to its increased vertical resolution and vastly reduced sampling times compared to traditional

205 snow pits. Indurated hoar in SMP profiles was more pronounced in the 2019 campaigns; well-defined layers were not as clearly visible in the SMP measurements from March 2018 (Fig. 2b), despite different layer densities being statistically separate in

the snowpit measurements, regardless of which year or when in the winter season the measurements were taken (Fig. 3). Throughout the course of the 2018 - 19 winter, slight increases in the density of wind slab and depth hoar layers occurred as the snowpack developed. Late season snow densities in both 2018 and 2019 were similar, with the exception of surface snow.

210   The density of this layer became more variable as each winter progressed due to the competing processes of wind compaction (increasing density) and metamorphism (decreasing density). The timing of sampling relative to fresh snowfall events, noted during both March campaigns, also influenced measured surface snow densities.

SMP density profiles were used to parameterise profiles of thermal conductivity for the full depth of the snowpack. Patterns in parametrized thermal conductivity profiles (Fig. 4) resemble those in SMP densities from which they were derived (Fig. 2b-

215   d). Surface snow thermal conductivities were low ($K_{eff-Sturm} \approx 0.1$ Wm^{-1} K^{-1}, $K_{eff-Calonne} \approx 0.2$ Wm^{-1} K^{-1}), but sharply increased with depth for the upper 5 % of the snowpack (Fig. 4b and c). Below this, at normalised depths of ~ 5 - 30 %, thermal conductivity reached maximum values ($K_{eff-Sturm} \approx 0.15$ Wm^{-1} K^{-1}, $K_{eff-Calonne} \approx 0.3$ Wm^{-1} K^{-1}). Between ~ 25 - 40 % normalised depth, thermal conductivity declined before stabilising at minimum values ($K_{eff-Sturm} \approx 0.1$ Wm^{-1} K^{-1}, $K_{eff-Calonne} \approx 0.2$ Wm^{-1} K^{-1}) in the lower ~ 60 % of the snowpack. The Sturm et al. (1997) and Calonne et al. (2011) parameterisations showed similar

220   variation in thermal conductivity with depth, although the magnitude of values these parameterisations produced were shown to be statistically significantly different using a paired samples t-test in all three months ($t_{March2018} = 87.2$, $t_{Jan2019} = 39.5$, $t_{March2019}$ $= 38.9$); All statistical tests herein gave a p-value less than 0.001, denoting significance at the 99.9% level. Profiles of snowpack thermal conductivity were temporally consistent, with similar shape and values in January and March 2019. In March 2018, the amplitude of the thermal conductivity profiles was less pronounced than January and March 2019, particularly for the

225   parameterisation of Sturm et al. (1997). We recognise that the thermal conductivity of a snowpack is dependent on more than just its density (Sturm et al., 2002), with other factors such as snow microstructure and temperature also having an influence i.e. (Calonne et al., 2011) but these profiles still provide novel insights and a useful first-order approximation of snow heat transfer for model evaluation.

3.3 Modelled snowpack properties and comparison with observations

230   Simulated snow depths (Fig. 5a and d) were consistently lower than observations (from either Magnaprobe measurements (mean value) or the acoustic sounder depth on the 31 March at the AWS; Fig. 1b, Table 1). Timing of simulated snowpack accumulation leads to an effective snow depth in 2018 - 19 ($S_{depth,eff}CLM_{2018-19} = 66$ cm) more than double that in 2017 - 18 ($S_{depth,eff}CLM_{2017-18} = 24$ cm) with earlier snow onset allowing a greater degree of soil insulation. Simulated snow onset (11 October) and melt-out dates (25 May) were both approximately a week earlier than observed at the AWS in 2017 - 18; for the

235   following year the length of this offset was reduced to just one day. Observations of effective snow depth ($S_{depth,eff}Obs_{2017-18} = 57$ cm, $S_{depth,eff}Obs_{2018-19} = 101$ cm) similarly reflect greater insulation of the soil surface in 2018-19 compared to 2017-18.

Whilst the absolute number of simulated snow layers is plausible, their physical properties do not correspond to observations. The number and thickness of snow layers is result of overall snowpack depth. Figs. 5 b & e show three (or four) relatively homogenous layers, with a slight increase in density with depth. The highest mean (329 kg m^3) and median (340 kg m^3; Table

240   2) density are found in third snow layer (dark blue in Fig. 5).

This is in contrast to the three observed layers (surface snow, wind slab and depth hoar) consistently identified in the snowpit observations. Similar to other snow models (Domine et al., 2016; 2019) the physical characteristics of the depth hoar layer at the base of the snowpack (large faceted grains; low density) are not clearly distinct from an overlying wind slab layer (small rounded grains; high density).This is the result of the lack of representation ofdepth hoar layer development in CLM (Van

245   Kampenhout et al., 2017). These discrepancies between modelled and measured snow density and stratigraphy negatively impact the simulation of K_{eff}, as layer thermal conductivities were dependent on density of each layer (Eq. 2).

CLM overestimated the thermal conductivity of tundra snowpacks compared to in-situ measurements using needle probes or estimated from SMP profiles (Fig. 6a). Median simulated snow thermal conductivities (0.30 Wm^{-1} K^{-1}) were three times greater

than either needle probe measurements (0.08 Wm^{-1} K^{-1}) or SMP-derived estimates using the Sturm approximation (x$_{Keff-Sturm}$

250 = 0.11 Wm^{-1} K^{-1}), with the median thermal conductivity using the Calonne approximation still notably lower (x$_{Keff-Calonne}$ = 0.25 Wm^{-1} K^{-1}) than simulated thermal conductivities. SMP K$_{eff}$ parameterisation from Sturm et al. (1997; derived from measurements in Alaskan tundra snow), are closer to values from needle probe measurements than SMP K$_{eff}$ derived using Calonne et al. (2011) (Fig. 6a). The modelled thermal conductivity of simulated snow layers was relatively homogenous between layers in contrast to thermal conductivities derived from either the SMP (Fig. 4) or the needle probe measurements

255 (Table 2), with analysis of variance again only showing layers to significantly differ from the surface layer (F = 39.74). Needle probe measurements of the depth hoar layer had low thermal conductivities (0.05 Wm^{-1} K^{-1}), with a slight increase in mean thermal conductivity for indurated hoar (0.09 Wm^{-3} K^{-1}) and a further increase for the mean wind slab thermal conductivity (0.20 Wm^{-1} K^{-1}). Distributions of simulated snow thermal conductivities were statistically significantly different from all measurement methods at the 0.01 level using a Kruskal-Wallis test, as were those from the SMP using the Calonne

260 parameterization. Differences between the distribution of needle probe measurements and SMP with the Sturm parameterization were not statistically significant.

3.4 Simulated Soil Temperatures, Correction Factors and Snow Heat Transfer

Simulated soil temperatures were considerably colder than observations (RMSE = 5.0 ℃, Bias = - 2.2 ℃), especially during the maximum duration of simulated snow cover (15 Sept – 31 May; RMSE = 5.8 ℃). Reducing simulated snow thermal

265 conductivities led to warmer soil temperatures closer to observed values (Fig. 8.), as the snow more effectively insulated underlying soil which prevented heat from being released to the atmosphere. In order to improve thermal conductivity simulations, a multiplier (α) was applied to the ice content term in Eq. 1:

$$\rho = \frac{(\alpha \times m_i) \times m_{lw}}{F_{sno} \times h_{sl}} \qquad (3)$$

270

Although appearing to be a function of density, this multiplier is added separate from the calculation of layer snow densities, and only feeds into the calculation of snow thermal conductivity, and thus snow mass is conserved. Values of α were chosen which would reduce simulated densities to the range of observed values, with an α of 0.65 giving the K$_{eff}$ for snow with a density between the interquartile range of observed values shown in Table 2. A set of sensitivity tests were then carried out

275 where the value of α was iteratively changed from 0.75 to 0.25 in 0.05 increments (Fig. 6b). As the RMSE and the SHTM look at changes over slightly different time periods (RMSE = entire winter, SHTM = Oct – March), different metrics may imply different adjustments give the best model performance. In 2018-19, a value of α between 0.65 and 0.6 resulted in the optimal model performance (Figure 7), with a SHTM value of 0.991 (or 0.979) and a RMSE of 1.5 ℃ (or 1.2 ℃).

Reducing simulated snow density in Eq. 3 (0.55 ≤ α ≤ 0.3) below the lowest quartile of observed values was required to

280 increase soil temperatures to the observed range, particularly for 2017 – 18 where wintertime minimum soil temperatures are up to 12.8 ℃ warmer relative to the baseline model run (Fig. 8a). Using the same best-fit value of α for the entire model run can still give good model performance, with a maximum value for the SHTM of 0.987 for an α of 0.40, even though different α will better fit different years of the simulation. Errors in the timing and depth of simulated snow cover (Fig. 8b) impact the magnitude of insulation it provides, and thus the best-fit value of α (Fig. 9). A multiple linear regression was undertaken to

285 quantify the influence of snow depth and snow depth error on the value of the best fit correction factor, which showed errors in the simulated snow depth can be compensated by a greater adjustment to snow thermal conductivity (Fig 9b). Equation 4 was generated using data from both seasons for the period where snow cover was established in both the model and the observations up to and including peak simulated snow depth:

290
$$\alpha = 0.22 + 1.14S - 0.26E + 0.55SE \tag{4}$$

where S equals the simulated snow depth, and E equals the simulated snow depth error. Best fit correction values were strongly related to snow depth ($R^2 = 0.77$, RMSE = 0.066), with different values of α more appropriate for deep (> 25 cm, $\alpha \approx 0.6$) and shallow (< 15 cm, $\alpha \approx 0.3$) snow (Fig. 9a).

4 Discussion

4.1 Variability of thermal properties

SMP profiles, processed as detailed in Appendix A, produced snow layer densities closely matched to density cutter measurements at TVC (Fig. 3) and consistent with measurements from other Arctic and sub-Arctic environments, e.g. ρ_{SS} = ~ 100 kg m³, ρ_{WS} = 300 - 500 kg m³, ρ_{DH} = 150 - 250 kg m³ in Barrere et al. (2017); Benson and Sturm (1993); Derksen et al. (2014), Domine et al. (2002; 2012; 2016). SMP profiling has considerably increased the vertical resolution of density measurements and vastly reduced sampling times compared to traditional snowpits, enabling a far greater number of measurement profiles to be made across a wider distribution of snowpack conditions. Deriving profiles of thermal conductivity for the full depth of the snowpack, as facilitated by the SMP, is a novel approach, with most previous studies of snow thermal conductivity based on values sampled at a resolution of ~ 10 cm (Domine et al., 2012; 2015; 2016; Gouttevin et al., 2018; Morin et al., 2010).

Depth normalisation of SMP profiles (n > 200 per measurement campaign) allowed comparison of snow properties with varying absolute depth. Snow depth distributions from all campaigns matched the distribution shape and median values of tundra snow depths acquired across a ~ 1500 km traverse as described inDerksen et al. (2009), which may suggests transferability across wider Arctic tundra regions. Relative depth profiles of density at TVC remain consistent for all sampling campaigns, regardless of overall snowpack depth. Densities in the portion of the depth hoar layer located between 40 - 80 % depth were likely overestimated (although SMP estimates remain within the interquartile range of snowpit measurements) due to an assumption of heteroscedasticity made by the algorithm of Proksch et al. (2015), which may not apply for a material as anisotropic as depth hoar (Fig. A2). Additionally, pressure exerted on the ice matrix by the SMP may have caused wider collapse of the weak depth hoar structure during measurement. As a result, the force required to penetrate the snow may be reduced (potentially below the detection limit of the SMP) in the gaps where the ice matrix has collapsed; Required penetration force will conversely increase towards the base of the snowpack where the collapsed depth hoar has accumulated. This, plus an increased probability of SMP-vegetation interactions at the base of the snowpack, is likely the cause of density (and density-derived K_{eff}) increases in the lower ~ 20 % of all profiles. While exact impact of ice matrix collapse in depth hoar is not possible to quantify directly, this limitation is not without comparison in other direct, contact measurements of snow properties such as volumetric sampling of density (Conger and Mcclung, 2009; Proksch et al., 2016) and μ-CT (Zermatten et al., 2011). The higher vertical resolution of SMP density profiles (1.25 mm, or 0.25 % of snowpack depth) relative to traditional snowpit measurements (3 cm) allows snowpack features to be much more finely resolved (Calonne et al., 2020; King et al., 2020b; Proksch et al., 2015). Moving away from bulk sampling of layers with boundaries defined by abrupt binary transitions as identified by traditional stratigraphic techniques, to more continuous profiles enables features such as indurated hoar, typically a subtle transitional layer, to be captured and quantified (Pielmeier and Schneebeli, 2003; Proksch et al., 2016). Higher resolution measurements (μ-CT, SMP) of continuous profiles are increasingly implemented (e.g., Proksch et al. (2016); Calonne et al. (2020); Wagner et al. (2021)) but this conceptualisation of snow as a continuous profile rather than a series of discrete layers is not yet implemented in snowpack modelling, excepting the test case outlined by Simson et al. (2021).

4.2 Evaluation of snowpack and soil temperature simulations

330 Density profiles of Arctic snow from physical snow model simulations are inverted relative to observations, exhibiting low density snow in the upper part of the snowpack and high density snow at the base similar to what would be expected in taiga and alpine environments (Barrere et al., 2017; Domine et al., 2019). CLM is no exception, with the model producing four layers of uniformly high density snow, rather than a low density snow layer adjacent to the ground overlain by a higher density slab layer. Consequently, simulated density profiles are not representative of field measurements and the overall bulk density

335 of the snowpack is overestimated. This is common of other snow models of similar physical complexity, e.g. ISBA-ES (Barrere et al., 2017), and higher complexity, e.g. SNOWPACK (Bartelt and Lehning, 2001) and Crocus (Vionnet et al., 2012), because they do not account for vital arctic processes (Domine et al., 2016; 2019), such as the snowpack vapour kinetics, necessary to form depth hoar. As K_{eff} is simulated as a function of density, when models are unable to accurately describe the density profiles of Arctic snowpacks, this has a negative impact on how well K_{eff} can be simulated (Gouttevin et al., 2018). K_{eff} values

340 from CLM are not only overestimated relative to field measurements, but also in comparison to simulations from more complex snow models in similar environments (Barrere et al., 2017; Domine et al., 2019).

The impact of snow insulation on soil temperatures is dependent on both the depth and thermal conductivity of the snowpack (Gouttevin et al., 2012), as well as the timing of snow accumulation (Lafrenière et al., 2013). Changes to the simulated thermal conductivity improve modelled soil temperatures, although the magnitude of the required bias correction varies both

345 throughout the snow season and interannually depending on how well snow depths are simulated. This is particularly important at the start of the snow season when erroneous modelled heat exchanges between air, snow and soil influence soil and snowpack properties and development, and are carried forward until the end of the snow season (Sandells et al., 2012). In particular, simulations are sensitive to latent heat release during soil freeze-up, which maintains soil temperatures close to 0 °C for an extended period of time at the beginning of the winter (Yi et al., 2019). Temperature differences between soil and air induce a

350 strong snowpack temperature gradient, leading to depth hoar formation and thus determining the structure of the snowpack and its capacity to insulate the soil (Domine et al., 2018).

4.3 Impact of correction factors on heat transfer

Values of the SHTM increase by up to 0.3 as a result of applying the correction factor (Fig. 7), where the best-fit value of α gives the highest SHTM for a particular year. Ignoring interannual variability and calculating one SHTM value (SHTM =

355 0.733) for the entire model run (Slater et al., 2017) suggests far more accurate simulation of soil temperatures from the baseline model run than seen in Fig. 8a, outperforming 8 of the 13 models in Slater et al. (2017). Prescribing simulated snow thermal conductivity to a more physically representative value leads to a notable improvement in simulating soil temperatures in tundra environments, compared to both the findings herein and the permafrost model used in Yi et al. (2020). Cook et al. (2007) also found that reducing simulated snow thermal conductivity to the lower end of observed values reduced soil temperature biases

360 in an older version of CLM (CLM3.0).

Improving model performance during the soil freeze-up period is vital to accurately model soil temperatures for the entirety of the winter. Differences between absolute and effective snow depths from both the model and the observational record also highlight the importance of the early season snowpack in regulating soil temperatures for the entire snow season. Larger values of the correction factor are needed to replicate observed soil temperatures later in the winter season, as errors in simulating

365 earlier season snow depth are additive, leading to larger discrepancies for both snow depth and soil temperatures.

The impact of differences between simulated and observed snow depth can be compensated by a greater adjustment to snow thermal conductivity. This bias compensation between underestimates of snow depth and overestimates of snow thermal conductivity is also seen in other land surface models, e.g. JULES, LPJ-GUESS (Wang et al., 2016). A stronger correction is needed when snow cover is below ~ 25 cm, potentially indicative of a degree of insulation saturation, as has been previously

370 suggested (Lawrence and Slater, 2009; Slater et al., 2017; Zhang, 2005). Shallow snowpacks are likely to consist of a lower proportion of wind slab (Rutter et al., 2019) and thus their microstructural properties are less accurately represented by CLM, which does not simulate depth hoar (Van Kampenhout et al., 2017), stipulating the need for a larger adjustment to α. Multiple linear regression shows CLM to be reasonably insensitive to errors in simulated snow depth, thus future applications can use simulated snow depths in order to approximate a sensible value for the correction factor even if no measurement of snow depth

375 is available.

Ekici et al. (2015) suggested that representation of snow thermal conductivity in land surface models is less important for accurate simulation of soil temperatures than other processes not currently well represented in most land surface schemes, such as blowing snow and depth hoar formation. Reducing simulated thermal conductivity by 80 % ($\alpha = 0.3$) produces changes in soil temperatures approximately equivalent to the impact of changing depth hoar fraction from 0 to 60 % (Zhang et al., 1996),

380 suggesting the inclusion of vapour transport in the snowpack is at least equally important as values of snow thermal conductivity in accurately simulating wintertime soil temperatures. Further improvements in SHTM in future iterations of CLM will require a physically representative approach to snow density and thermal conductivity through explicit inclusion of vapour transport within the snowpack, currently under development in stand-alone snow microphysical models (Fourteau et al., 2021; Jafari et al., 2020; Schürholt et al., 2021). Meanwhile, an empirically derived scaling factor as shown above provides

385 a computationally efficient compromise, reducing both the value of K_{eff} and the cold bias of simulated wintertime soil temperatures considerably (RMSE reduction of 3.7 °C for $\alpha = 0.45$). Model underestimates of soil temperatures follow through into calculations of soil respiration, further contributing to uncertainties surrounding estimates of wintertime carbon flux (Natali et al. 2019) and suggesting that such modelled values are likely to be an underestimation of the true magnitude of these fluxes. Being able to accurately model fluxes outside of the growing season is important as these make a considerable

390 contribution to the annual carbon budget (Natali et al 2019; Schuur et al 2021). A low soil temperature bias due to poorly simulated snow insulation also has consequences for predicting the evolution of permafrost (Barrere et al., 2017; Burke et al., 2020) and resultant carbon emissions as this degrades (Peng et al., 2016).

5 Conclusions

A new recalibration to derive profiles of snow density and thermal conductivity from SMP profiles of penetration force is

395 presented, with resulting densities and thermal conductivities then used to evaluate the performance of CLM5.0 and derive scaling factors to improve simulated soil temperature. SMP-derived density profiles show good agreement with measured snow layer densities at TVC. Comparison of measured snowpack properties from in situ SMP and needle probe techniques with simulations show the model tends to overestimate snow layer thermal conductivities by a up to factor of three, with implications for how well wintertime soil temperatures are simulated. Reducing simulated thermal conductivities improves

400 simulation of soil temperature (RMSE reduction of 3.7 °C). The optimal magnitude of this reduction is strongly linked to snow depth, with a greater reduction needed for shallower snowpacks.

Further improvements to simulated snow properties will require more explicit representation of key processes not currently accounted for in CLM, chiefly the formation of depth hoar. A more physically representative snowpack should also improve simulation of wintertime soil thermal conditions. Snowpack vapour kinetics are not currently included within global land

405 surface models, which also have to consider a large variety of other processes and avenues for future development (Blyth et al., 2021; Fisher and Koven, 2020), although developments are being made to consider these in complex microscale snow physics models. Empirical scaling of snow thermal conductivity provides a computationally efficient interim solution with a similar impact on soil temperatures as the explicit representation of a large depth hoar fraction in point-scale simulations by Zhang et al. (1996). Improving the accuracy with which Arctic wintertime soil temperatures can be simulated may help to

410 reduce sizable uncertainties (Natali et al., 2019) surrounding current projections of wintertime carbon fluxes.

6 Appendix A: SMP Processing

Differences between study environments (the original SMP coefficients were not derived for tundra snow) and SMP hardware for different versions of the SMP used by Proksch et al. (2015) and this study required new coefficients to be derived in order to relate penetration force to density. Methods from King et al. (2020b) were adapted to recalibrate SMP measurements from

415 TVC in January and March 2019, described in detail in Fig. A1Co-incident SMP profiles and snowpit density measurements were available at 36 locations across the TVC catchment. A K-folds process is then used to derive new coefficients ($a - d$; Table A1) for Eq. A1 (Eq. 9 in Proksch et al. (2015)):

$$\rho_{SMP} = \boldsymbol{a} + \boldsymbol{b}ln(\tilde{F}) + \boldsymbol{c}ln(\tilde{F})L + \boldsymbol{d}L \qquad (A1)$$

420

where $\tilde{F}$ is the median force value over the vertical distance density is being calculated and L is the element size, the distance between points where force is exerted by the SMP - approximately the distance between snow grains (Löwe and Van Herwijnen, 2012). Individual pairs of SMP derived and snowpit measured densities above the 95th percentile of absolute error were removed (Fig. A1 – Step 7), and the K-folds recalibration repeated (Step 8) to produce revised coefficients to recalibrate

425 the entire SMP dataset (Step 9). This process was iterated until paired SMP-snowpit profiles with an R^2 of less than 0.7 were removed. Poor fitting between some paired SMP-snowpit profiles was due to the spatially heterogeneous nature of the snowpack (King et al., 2020b), as microtopographic variation in hummocky tundra can lead to considerable sub-metre snowpack variability. Coefficients (Table A1) were ultimately derived from 21 paired SMP-snowpit density profiles; 16 from the January 2019 campaign, and 5 from the March 2019 campaign ($R^2 = 0.88$, $p < 0.001$). These coefficients give a RMSE of

430 25.2, compared to an RMSE of 125 for those of Proksch et al. (2015).

These coefficients were used to calculate density profiles for all 640 profiles from the 2019 campaigns (Fig. A1 – Step 12). Densities for SMP profiles from the March 2018 campaign were also derived from these, but measurements from this campaign were not included in the recalibration dataset. Metrics were calculated over a 2.5mm sliding window with 50 % overlap, (ie. 1.25mm resolution) as per Proksch et al. (2015). Profiles of thermal conductivity were then calculated from SMP densities,

435 using the density: K_{eff} relationships derived by Sturm et al. (1997) and Calonne et al. (2011) (Fig. A1 - Step 17). It is important to note that the thermal conductivity of a snowpack is dependent on more than just its density (Sturm et al., 2002), but these parameterisations provide a useful first-order approximation.

Prior to recalibration, negative force values were removed from the SMP profiles. These are erroneous values which can occur in the SMP output when ice gets caught in the cog wheel of the SMP or if part of the instrument is damaged (Lutz, 2009).

440 Buried vegetation may also be present in the lower part of tundra snowpacks, and interaction between SMP and dense shrubs or branches may cause the SMP signal to overload and affect the quality of lower sections of the profile. A normalised percentage depth scale (with profiles rescaled to a resolution of 0.25 % of total depth using linear interpolation) was used to compare SMP-derived profiles of density and K_{eff} from different snow depths (Steps 15 and 18). Any negative densities or thermal conductivities were removed during the depth normalisation process.

445 Recalibrated density profiles from the SMP do not produce values below 200 kg m^3, despite observations of lower snow densities in Arctic depth hoar, including some from this campaign (Fig. 2). Figure A2b shows a large spread in the value of L for the depth hoar samples, over a relatively small set of snowpit densities. Large element sizes, or distances between snow grain failures, are not unexpected in depth hoar but this results in a low signal to noise ratio (King et al., 2020b). Figure A2c shows the relationship between $\tilde{F}$ and L is not heteroscedastic as initially assumed, leading to an overestimation of the density

450 (and density-derived K_{eff}) of this layer. Proksch et al. (2015) state that their model does not yet fully account for the anisotropic structure of some snow types, which is of particular relevance to depth hoar.

7 Appendix B: Model Spin-up

In order to determine the amount of model spin-up required for soil temperatures to equilibrate, iterative runs of PTCLM with an additional year of spin-up were undertaken from 1 January 2017 to 1 January 2013. Soil temperatures throughout the soil

455 column were compared; 3 depths are shown in Fig. B1. Internal system variability results in a difference of ~ 1 °C between model runs, with a minimum of 2 years of spin-up required for K_{eff} adjusted runs to converge at a 10cm soil depth. Deviation between different spin-up start times takes longer to level out deeper in the soil column, but as we only examine soil properties within the top 20cm of the soil column, we feel this length of spin-up is sufficient. Changes to snow thermal conductivity were evident at all depths in the soil profile, and have an impact on the thickness of the active layer with seasonal thawing seen to a

460 depth of 1.7 m (Fig. B1b), in comparison to 1.35 m for the unadjusted CLM runs and the 1 m active layer depth reported by Grünberg et al. (2020).

Code & Data availability

Code and data to produce figures is available at: https://github.com/V-Dutch/TVCSnowCLM

Author Contribution

465 Investigation, Formal Analysis, Writing - Original Draft preparation; VRD. Supervision; NR, LW, MS, CD, RK. Data acquisition; NR, CD, RE, JK (TVC Snow Data); BW, GHG, OS (TVC Meteorological Observations). Data Planning; PM. Software; JK, MS (SMP); LW (CLM). Funding acquisition; NR. All authors were involved in reviewing and editing prior to submission.

Competing Interests

470 Some authors are members of the editorial board of The Cryosphere. The peer-review process was guided by an independent editor, and the authors have also no other competing interests to declare

Acknowledgements

VRD was funded by an RDF Studentship from Northumbria University and the Northern Water Futures project. This project was conducted with approval issued by Aurora Research Institute– Aurora College (License Nos. 16237 & 16501). The authors

475 would like to acknowledge that this study occurred within the Inuvialuit Settlement Region located in the Western Canadian Arctic.

References

480 Anderson, E., A.: A point energy and mass balance model of a snow cover, National Oceanic and Atmospheric Administration, Silver Spring, Maryland, 1976.

Barrere, M., Domine, F., Decharme, B., Morin, S., Vionnet, V., and Lafaysse, M.: Evaluating the performance of coupled snow–soil models in SURFEXv8 to simulate the permafrost thermal regime at a high Arctic site, Geoscientific Model Development, 10, 3461-3479, 10.5194/gmd-10-3461-2017, 2017.

485 Bartelt, P. and Lehning, M.: A physical SNOWPACK model for the Swiss avalanche warning Part I: numerical model, Cold Regions Science and Technology, 35, 123-145, 10.1016/S0165-232X(02)00074-5, 2001.

Benson, C. S. and Sturm, M.: Structure and wind transport of seasonal snow on the Arctic slope of Alaska, Annals of Glaciology, 18, 261-267, 10.3189/s0260305500011629, 1993.

Biskaborn, B. K., Smith, S. L., Noetzli, J., Matthes, H., Vieira, G., Streletskiy, D. A., Schoeneich, P., Romanovsky, V. E., Lewkowicz, A.
490 G., Abramov, A., Allard, M., Boike, J., Cable, W. L., Christiansen, H. H., Delaloye, R., Diekmann, B., Drozdov, D., Etzelmuller, B., Grosse, G., Guglielmin, M., Ingeman-Nielsen, T., Isaksen, K., Ishikawa, M., Johansson, M., Johannsson, H., Joo, A., Kaverin, D., Kholodov, A., Konstantinov, P., Kroger, T., Lambiel, C., Lanckman, J. P., Luo, D., Malkova, G., Meiklejohn, I., Moskalenko, N., Oliva, M., Phillips, M., Ramos, M., Sannel, A. B. K., Sergeev, D., Seybold, C., Skryabin, P., Vasiliev, A., Wu, Q., Yoshikawa, K., Zheleznyak, M., and Lantuit, H.: Permafrost is warming at a global scale, Nat Commun, 10, 264, 10.1038/s41467-018-08240-4, 2019.

495 Blyth, E. M., Arora, V. K., Clark, D. B., Dadson, S. J., De Kauwe, M. G., Lawrence, D. M., Melton, J. R., Pongratz, J., Turton, R. H., Yoshimura, K., and Yuan, H.: Advances in Land Surface Modelling, Current Climate Change Reports, 7, 45-71, 10.1007/s40641-021-00171-5, 2021.

Burke, E. J., Zhang, Y., and Krinner, G.: Evaluating permafrost physics in the Coupled Model Intercomparison Project 6 (CMIP6) models and their sensitivity to climate change, The Cryosphere, 14, 3155-3174, 10.5194/tc-14-3155-2020, 2020.

500 Calonne, N., Flin, F., Morin, S., Lesaffre, B., du Roscoat, S. R., and Geindreau, C.: Numerical and experimental investigations of the effective thermal conductivity of snow, Geophysical Research Letters, 38, 10.1029/2011gl049234, 2011.

Calonne, N., Richter, B., Löwe, H., Cetti, C., ter Schure, J., Van Herwijnen, A., Fierz, C., Jaggi, M., and Schneebeli, M.: The RHOSSA campaign: multi-resolution monitoring of the seasonal evolution of the structure and mechanical stability of an alpine snowpack, The Cryosphere, 14, 1829-1848, 10.5194/tc-14-1829-2020, 2020.

505 Conger, S. M. and McClung, D. M.: Comparison of density cutters for snow profile observations, Journal of Glaciology, 55, 163-169, 2009.

Cook, B. I., Bonan, G. B., Levis, S., and Epstein, H. E.: The thermoinsulation effect of snow cover within a climate model, Climate Dynamics, 31, 107-124, 10.1007/s00382-007-0341-y, 2007.

Dai, Y. and Zeng, Q.: A Land Surface Model (IAP94) for Climate Studies - Part I: Formulation and Validation in Off-line experiments, Advances in Atmospheric Sciences, 14, 432-460, 1997.

510 Derksen, C., Lemmetyinen, J., Toose, P., Silis, A., Pulliainen, J., and Sturm, M.: Physical properties of Arctic versus subarctic snow: Implications for high latitude passive microwave snow water equivalent retrievals, Journal of Geophysical Research: Atmospheres, 119, 7254-7270, 10.1002/2013jd021264, 2014.

Derksen, C., Sturm, M., Holmgren, J., Liston, G. E., Huntington, H., Silis, A., and Solie, D.: Northwest Territories and Nunavut Snow Characteristics from a Subarctic Traverse: Implications for Passive Microwave Remote Sensing, Journal of Hydrometeorology, 10, 448-
515 463, 10.1175/2008jhm1074.1, 2009.

Domine, F., Barrere, M., and Sarrazin, D.: Seasonal evolution of the effective thermal conductivity of the snow and the soil in high Arctic herb tundra at Bylot Island, Canada, The Cryosphere, 10, 2573-2588, 10.5194/tc-10-2573-2016, 2016.

Domine, F., Cabanes, A., and Legagneux, L.: Structure, microphysics, and surface area of the Arctic snowpack near Alert during the ALERT 2000 campaign, Atmospheric Environment, 36, 2753-2765, 2002.

520 Domine, F., Gallet, J.-C., Bock, J., and Morin, S.: Structure, specific surface area and thermal conductivity of the snowpack around Barrow, Alaska, Journal of Geophysical Research: Atmospheres, 117, n/a-n/a, 10.1029/2011jd016647, 2012.

Domine, F., Barrere, M., Sarrazin, D., Morin, S., and Arnaud, L.: Automatic monitoring of the effective thermal conductivity of snow in a low-Arctic shrub tundra, The Cryosphere, 9, 1265-1276, 10.5194/tc-9-1265-2015, 2015.

Domine, F., Belke-Brea, M., Sarrazin, D., Arnaud, L., Barrere, M., and Poirier, M.: Soil moisture, wind speed and depth hoar formation in
525 the Arctic snowpack, Journal of Glaciology, 64, 990-1002, 10.1017/jog.2018.89, 2018.

Domine, F., Picard, G., Morin, S., Barrere, M., Madore, J.-B., and Langlois, A.: Major Issues in Simulating Some Arctic Snowpack Properties Using Current Detailed Snow Physics Models: Consequences for the Thermal Regime and Water Budget of Permafrost, Journal of Advances in Modeling Earth Systems, 11, 34-44, 10.1029/2018ms001445, 2019.

Ekici, A., Chadburn, S., Chaudhary, N., Hajdu, L. H., Marmy, A., Peng, S., Boike, J., Burke, E., Friend, A. D., Hauck, C., Krinner, G.,
530 Langer, M., Miller, P. A., and Beer, C.: Site-level model intercomparison of high latitude and high altitude soil thermal dynamics in tundra and barren landscapes, The Cryosphere, 9, 1343-1361, 10.5194/tc-9-1343-2015, 2015.

Essery, R. and Pomeroy, J.: Vegetation and Topographic Control of Wind-Blown Snow Distributions in Distributed and Aggregated Simulations for an Arctic Tundra Basin, Journal of Hydrometeorology, 5, 735-744, 2004.

Essery, R., Kontu, A., Lemmetyinen, J., Dumont, M., and Ménard, C. B.: A 7-year dataset for driving and evaluating snow models at an
535 Arctic site (Sodankylä, Finland), Geoscientific Instrumentation, Methods and Data Systems, 5, 219-227, 10.5194/gi-5-219-2016, 2016.

Fierz, C., Armstrong, R. L., Durand, Y., Etchevers, P., Greene, E., McClung, D. M., Nishimura, K., Satyawali, P. K., and Sokratov, S. A.: The International Classification for Seasonal Snow on the ground, 2009.

Fisher, J. B., Sikka, M., Oechel, W. C., Huntzinger, D. N., Melton, J. R., Koven, C. D., Ahlström, A., Arain, M. A., Baker, I., Chen, J. M., Ciais, P., Davidson, C., Dietze, M., El-Masri, B., Hayes, D., Huntingford, C., Jain, A. K., Levy, P. E., Lomas, M. R., Poulter, B., Price, D.,
540 Sahoo, A. K., Schaefer, K., Tian, H., Tomelleri, E., Verbeeck, H., Viovy, N., Wania, R., Zeng, N., and Miller, C. E.: Carbon cycle uncertainty in the Alaskan Arctic, Biogeosciences, 11, 4271-4288, 10.5194/bg-11-4271-2014, 2014.

Fisher, R. A. and Koven, C. D.: Perspectives on the Future of Land Surface Models and the Challenges of Representing Complex Terrestrial Systems, Journal of Advances in Modeling Earth Systems, 12, 10.1029/2018ms001453, 2020.

545   Fourteau, K., Domine, F., and Hagenmuller, P.: Macroscopic water vapor diffusion is not enhanced in snow, The Cryosphere, 15, 389-406, 10.5194/tc-15-389-2021, 2021.

Goncharova, O. Y., Matyshak, G. V., Epstein, H. E., Sefilian, A. R., and Bobrik, A. A.: Influence of snow cover on soil temperatures: Meso- and micro-scale topographic effects (a case study from the northern West Siberia discontinuous permafrost zone), Catena, 183, 10.1016/j.catena.2019.104224, 2019.

550   Gouttevin, I., Langer, M., Löwe, H., Boike, J., Proksch, M., and Schneebeli, M.: Observation and modelling of snow at a polygonal tundra permafrost site: spatial variability and thermal implications, The Cryosphere, 12, 3693-3717, 10.5194/tc-12-3693-2018, 2018.

Gouttevin, I., Menegoz, M., Dominé, F., Krinner, G., Koven, C., Ciais, P., Tarnocai, C., and Boike, J.: How the insulating properties of snow affect soil carbon distribution in the continental pan-Arctic area, Journal of Geophysical Research: Biogeosciences, 117, n/a-n/a, 10.1029/2011jg001916, 2012.

Gray, D. M. and Male, D. H.: Handbook of Snow: Principles, Processes, Management & Use, Blackburn Press, Caldwell, New Jersey1981.

555   Grünberg, I., Wilcox, E. J., Zwieback, S., Marsh, P., and Boike, J.: Linking tundra vegetation, snow, soil temperature, and permafrost, Biogeosciences, 17, 4261-4279, 10.5194/bg-17-4261-2020, 2020.

Hersbach, H., Bell, B., Berrisford, P., Hirahara, S., Horányi, A., Muñoz-Sabater, J., Nicolas, J., Peubey, C., Radu, R., Schepers, D., Simmons, A., Soci, C., Abdalla, S., Abellan, X., Balsamo, G., Bechtold, P., Biavati, G., Bidlot, J., Bonavita, M., Chiara, G., Dahlgren, P., Dee, D., Diamantakis, M., Dragani, R., Flemming, J., Forbes, R., Fuentes, M., Geer, A., Haimberger, L., Healy, S., Hogan, R. J., Hólm, E., Janisková,
560   M., Keeley, S., Laloyaux, P., Lopez, P., Lupu, C., Radnoti, G., Rosnay, P., Rozum, I., Vamborg, F., Villaume, S., and Thépaut, J. N.: The ERA5 global reanalysis, Quarterly Journal of the Royal Meteorological Society, 146, 1999-2049, 10.1002/qj.3803, 2020.

Jafari, M., Gouttevin, I., Couttet, M., Wever, N., Michel, A., Sharma, V., Rossmann, L., Maass, N., Nicolaus, M., and Lehning, M.: The Impact of Diffusive Water Vapor Transport on Snow Profiles in Deep and Shallow Snow Covers and on Sea Ice, Frontiers in Earth Science, 8, 10.3389/feart.2020.00249, 2020.

565   Jafarov, E. E., Nicolsky, D. J., Romanovsky, V. E., Walsh, J. E., Panda, S. K., and Serreze, M. C.: The effect of snow: How to better model ground surface temperatures, Cold Regions Science and Technology, 102, 63-77, 10.1016/j.coldregions.2014.02.007, 2014.

Jordan, R.: A One-Dimensional Temperature Model for a Snow Cover - Technical Documentation for SNTHERM.89, 1991.

King, J., Toose, P., Silis, A., and Derksen, C.: TVC Snow 2018-2019 tundra snow depth probe measurements (Version 1) [dataset], http://doi.org/10.5281/zenodo.4021401, 2020a.

570   King, J., Howell, S., Brady, M., Toose, P., Derksen, C., Haas, C., and Beckers, J.: Local-scale variability of snow density on Arctic sea ice, The Cryosphere Discussions, 10.5194/tc-2019-305, 2020b.

King, J., Derksen, C., Toose, P., Langlois, A., Larsen, C., Lemmetyinen, J., Marsh, P., Montpetit, B., Roy, A., Rutter, N., and Sturm, M.: The influence of snow microstructure on dual-frequency radar measurements in a tundra environment, Remote Sensing of Environment, 215, 242-254, 10.1016/j.rse.2018.05.028, 2018.

575   Koven, C., Riley, W. J., and Stern, A.: Analysis of Permafrost Thermal Dynamics and Response to Climate Change in the CMIP5 Earth System Models, Journal of Climate, 26, 1877-1900, 10.1175/JCLI-D-12-00228.1, 2012.

Lafrenière, M. J., Laurin, E., and Lamoureux, S. F.: The Impact of Snow Accumulation on the Active Layer Thermal Regime in High Arctic Soils, Vadose Zone Journal, 12, 10.2136/vzj2012.0058, 2013.

Lawrence, D. M. and Slater, A. G.: The contribution of snow condition trends to future ground climate, Climate Dynamics, 34, 969-981,
580   10.1007/s00382-009-0537-4, 2009.

Lawrence, D. M., Fisher, R. A., Koven, C., Oleson, K., Swenson, S., Vertenstein, M., Andre, B., Bonan, G., Ghimire, B., van Kampenhout, L., Kennedy, D., Kluzek, E., Knox, R., Lawrence, P., Li, F., Li, H., Lombardozzi, D., Lu, Y., Perket, J., Riley, W. J., Sacks, W. J., Shi, M., Wieder, W. R., Xu, C., Ali, A. A., Badger, A. M., Bisht, G., Broxton, P. D., Brunke, M. A., Buzan, J., Clark, M., Craig, T., Dahlin, K., Drewniak, B., Emmons, L., Fisher, J. B., Flanner, M., Gentine, P., Lenaerts, J., Levis, S., Leung, L. R., Lipscomb, W. H., Pelletier, J. D.,
585   Ricciuto, D. M., Sanderson, B. M., Shuman, J., Slater, A., Subin, Z. M., Tang, J., Tawfik, A., Thomas, Q., Tilmes, S., Vitt, F., and Zeng, X.: Technical Description of version 5.0 of the Community Land Model (CLM), National Centre for Atmospheric Research, Boulder, Colorado, 2018.

Lawrence, D. M., Fisher, R. A., Koven, C. D., Oleson, K. W., Swenson, S. C., Bonan, G., Collier, N., Ghimire, B., Kampenhout, L., Kennedy, D., Kluzek, E., Lawrence, P. J., Li, F., Li, H., Lombardozzi, D., Riley, W. J., Sacks, W. J., Shi, M., Vertenstein, M., Wieder, W. R., Xu, C.,
590   Ali, A. A., Badger, A. M., Bisht, G., Broeke, M., Brunke, M. A., Burns, S. P., Buzan, J., Clark, M., Craig, A., Dahlin, K., Drewniak, B., Fisher, J. B., Flanner, M., Fox, A. M., Gentine, P., Hoffman, F., Keppel-Aleks, G., Knox, R., Kumar, S., Lenaerts, J., Leung, L. R., Lipscomb, W. H., Lu, Y., Pandey, A., Pelletier, J. D., Perket, J., Randerson, J. T., Ricciuto, D. M., Sanderson, B. M., Slater, A., Subin, Z. M., Tang, J., Thomas, R. Q., Val Martin, M., and Zeng, X.: The Community Land Model Version 5: Description of New Features, Benchmarking, and Impact of Forcing Uncertainty, Journal of Advances in Modeling Earth Systems, 11, 4245-4287, 10.1029/2018ms001583, 2019.

595   Löwe, H. and van Herwijnen, A.: A Poisson shot noise model for micro-penetration of snow, Cold Regions Science and Technology, 70, 62-70, 10.1016/j.coldregions.2011.09.001, 2012.

Lutz, E. R.: Spatial and Temporal Analysis of Snowpack Strength and Stablity and Environmental Determinants on an Inclined, Forest Opening, Department of Earth Science, Montana State University, Bozeman, 2009.

Malle, J., Rutter, N., Webster, C., Mazzotti, G., Wake, L., and Jonas, T.: Effect of Forest Canopy Structure on Wintertime Land Surface
600   Albedo: Evaluating CLM5 Simulations With InSitu Measurements, Journal of Geophysical Research: Atmospheres, 10.1029/2020JD034118, 2021.

Marsh, P. and Pomeroy, J. W.: Spatial and temporal variations in snowmelt runoff chemistry, Northwest Territories, Canada, Water Resources Research, 35, 1559-1567, 10.1029/1998wr900109, 1999.

Marsh, P., Pomeroy, J., Pohl, S., Quinton, W., Onclin, C., Russell, M., Neumann, N., Pietroniro, A., Davison, B., and McCartney, S.:
605   Snowmelt Processes and Runoff at the Arctic Treeline: Ten Years of MAGS Research, in: Cold Region Atmospheric and Hydrologic Studies. The Mackenzie GEWEX Experience, 97-123, 10.1007/978-3-540-75136-6_6, 2008.

Morin, S., Domine, F., Arnaud, L., and Picard, G.: In-situ monitoring of the time evolution of the effective thermal conductivity of snow, Cold Regions Science and Technology, 64, 73-80, 10.1016/j.coldregions.2010.02.008, 2010.

Natali, S. M., Watts, J. D., Rogers, B. M., Potter, S., Ludwig, S. M., Selbmann, A.-K., Sullivan, P. F., Abbott, B. W., Arndt, K. A., Birch,
610   L., Björkman, M. P., Bloom, A. A., Celis, G., Christensen, T. R., Christiansen, C. T., Commane, R., Cooper, E. J., Crill, P., Czimczik, C., Davydov, S., Du, J., Egan, J. E., Elberling, B., Euskirchen, E. S., Friborg, T., Genet, H., Göckede, M., Goodrich, J. P., Grogan, P., Helbig, M., Jafarov, E. E., Jastrow, J. D., Kalhori, A. A. M., Kim, Y., Kimball, J. S., Kutzbach, L., Lara, M. J., Larsen, K. S., Lee, B.-Y., Liu, Z., Loranty, M. M., Lund, M., Lupascu, M., Madani, N., Malhotra, A., Matamala, R., McFarland, J., McGuire, A. D., Michelsen, A., Minions, C., Oechel, W. C., Olefeldt, D., Parmentier, F.-J. W., Pirk, N., Poulter, B., Quinton, W., Rezanezhad, F., Risk, D., Sachs, T., Schaefer, K.,
615   Schmidt, N. M., Schuur, E. A. G., Semenchuk, P. R., Shaver, G., Sonnentag, O., Starr, G., Treat, C. C., Waldrop, M. P., Wang, Y., Welker,

J., Wille, C., Xu, X., Zhang, Z., Zhuang, Q., and Zona, D.: Large loss of CO2 in winter observed across the northern permafrost region, Nature Climate Change, 9, 852-857, 10.1038/s41558-019-0592-8, 2019.

Niu, G.-Y. and Yang, Z.-L.: Effects of Frozen Soil on Snowmelt Runoff and Soil Water Storage at a Continental Scale, Journal of Hydrometeorology, 7, 937-952, 2006.

620 Pan, X., Yang, D., Li, Y., Barr, A., Helgason, W., Hayashi, M., Marsh, P., Pomeroy, J., and Janowicz, R. J.: Bias corrections of precipitation measurements across experimental sites in different ecoclimatic regions of western Canada, The Cryosphere, 10, 2347-2360, 10.5194/tc-10-2347-2016, 2016.

Peng, S., Ciais, P., Krinner, G., Wang, T., Gouttevin, I., McGuire, A. D., Lawrence, D., Burke, E., Chen, X., Decharme, B., Koven, C., MacDougall, A., Rinke, A., Saito, K., Zhang, W., Alkama, R., Bohn, T. J., Delire, C., Hajima, T., Ji, D., Lettenmaier, D. P., Miller, P. A.,

625 Moore, J. C., Smith, B., and Sueyoshi, T.: Simulated high-latitude soil thermal dynamics during the past 4 decades, The Cryosphere, 10, 179-192, 10.5194/tc-10-179-2016, 2016.

Pielmeier, C. and Schneebeli, M.: Developments in the Stratigraphy of Snow, Surveys in Geophysics, 24, 389-416, 2003.

Pomeroy, J., Marsh, P., and Lesack, L.: Relocation of Major Ions in Snow along the Tundra-Taiga Ecotone, Nordic Hydrology, 24, 151-168, 1993.

630 Proksch, M., Löwe, H., and Schneebeli, M.: Density, specific surface area, and correlation length of snow measured by high-resolution penetrometry, Journal of Geophysical Research: Earth Surface, 120, 346-362, 10.1002/2014jf003266, 2015.

Proksch, M., Rutter, N., Fierz, C., and Schneebeli, M.: Intercomparison of snow density measurements: bias, precision, and vertical resolution, The Cryosphere, 10, 371-384, 10.5194/tc-10-371-2016, 2016.

Quinton, W. L. and Marsh, P.: The Influence of Mineral Earth Hummocks on Subsurface Drainage in the Continuous Permafrost Zone,

635 Permafrost and Periglacial Processes, 9, 213-228, 1998.

Quinton, W. L. and Marsh, P.: A Conceptual Framework for Runoff Generation in a Permafrost Environment, Hydrological Processes, 13, 2563-2581, 1999.

Rees, A., English, M., Derksen, C., Toose, P., and Silis, A.: Observations of late winter Canadian tundra snow cover properties, Hydrological Processes, 28, 3962-3977, 10.1002/hyp.9931, 2014.

640 Riche, F. and Schneebeli, M.: Thermal conductivity of snow measured by three independent methods and anisotropy considerations, The Cryosphere, 7, 217-227, 10.5194/tc-7-217-2013, 2013.

Rutter, N., Sandells, M. J., Derksen, C., King, J., Toose, P., Wake, L., Watts, T., Essery, R., Roy, A., Royer, A., Marsh, P., Larsen, C., and Sturm, M.: Effect of snow microstructure variability on Ku-band radar snow water equivalent retrievals, The Cryosphere, 10.5194/tc-2019-167, 2019.

645 Sandells, M. J., Flerchinger, G. N., Gurney, R. J., and Marks, D.: Simulation of snow and soil water content as a basis for satellite retrievals, Hydrology Research, 43, 720-735, 10.2166/nh.2012.028, 2012.

Schneebeli, M. and Johnson, J. B.: A constant-speed penetrometer for high-resolution snow stratigraphy, Annals of Glaciology, 26, 107-111, 1998.

Schürholt, K., Kowalski, J., and Löwe, H.: Elements of future snowpack modeling - part 1: A physical instability arising from the non-linear

650 coupling of transport and phase changes, The Cryosphere Discussions, 10.5194/tc-2021-72, 2021.

Semenchuk, P. R., Elberling, B., Amtorp, C., Winkler, J., Rumpf, S., Michelsen, A., and Cooper, E. J.: Deeper snow alters soil nutrient availability and leaf nutrient status in high Arctic tundra, Biogeochemistry, 124, 81-94, 10.1533/s10533-015-0082-7, 2015.

Simson, A., Löwe, H., and Kowalski, J.: Elements of future snowpack modeling - part 2: A modular and extendable Eulerian–Lagrangian numerical scheme for coupled transport, phase changes and settling processes, The Cryosphere Discussions, 10.5194/tc-2021-73, 2021.

655 Slater, A. G., Lawrence, D. M., and Koven, C. D.: Process-level model evaluation: a snow and heat transfer metric, The Cryosphere, 11, 989-996, 10.5194/tc-11-989-2017, 2017.

Smith, C. D.: Correcting the Wind Bias in Snowfall Measurements Made with a Geonor T-200B Precipitation Gauge and Alter Wind Shield, Bulletin of the Canadian and Oceanographic Meteorological Society, 36, 162-167, 2008.

Sturm, M. and Holmgren, B.: An Automatic Snow Depth Probe for Field Validation Campaigns, Water Resources Research, 54, 9695-9701,

660 10.1029/2018WR023559, 2018.

Sturm, M., Holmgren, J., and Liston, G. E.: A Seasonal Snow Cover Classification for Local to Global Applications, Journal of Climate, 8, 1261-1283, 1995.

Sturm, M., Perovich, D. K., and Holmgren, J.: Thermal conductivity and heat transfer through the snow on the ice of the Beaufort Sea, Journal of Geophysical Research, 107, 10.1029/2000jc000409, 2002.

665 Sturm, M., Holmgren, J., Konig, M., and Morris, K.: The thermal conductivity of seasonal snow, Journal of Glaciology, 43, 26-41, 1997.

Sullivan, P. F., Welker, J. M., Arens, S. J. T., and Sveinbjörnsson, B.: Continuous estimates of CO2 efflux from arctic and boreal soils during the snow-covered season in Alaska, Journal of Geophysical Research: Biogeosciences, 113, 10.1029/2008jg000715, 2008.

Swenson, S. C. and Lawrence, D. M.: A new fractional snow-covered area parameterization for the Community Land Model and its effect on the surface energy balance, Journal of Geophysical Research: Atmospheres, 117, n/a-n/a, 10.1029/2012jd018178, 2012.

670 Taylor, K. E., Stouffer, R. J., and Meehl, G. A.: An Overview of CMIP5 and the Experiment Design, Bulletin of the American Meteorological Society, 93, 485-498, 10.1175/bams-d-11-00094.1, 2012.

Toose, P., King, J., Silis, A., and Derksen, C.: TVC Snow 2017-2018 tundra snow depth probe measurements (Version 1) [dataset], http://doi.org/10.5281/zenodo.4021328, 2020.

van Kampenhout, L., Lenaerts, J. T. M., Lipscomb, W. H., Sacks, W. J., Lawrence, D. M., Slater, A. G., and van den Broeke, M. R.:

675 Improving the Representation of Polar Snow and Firn in the Community Earth System Model, Journal of Advances in Modeling Earth Systems, 9, 2583-2600, 10.1002/2017ms000988, 2017.

Vionnet, V., Brun, E., Morin, S., Boone, A., Faroux, S., Le Moigne, P., Martin, E., and Willemet, J. M.: The detailed snowpack scheme Crocus and its implementation in SURFEX v7.2, Geoscientific Model Development, 5, 773-791, 10.5194/gmd-5-773-2012, 2012.

Virkkala, A. M., Aalto, J., Rogers, B. M., Tagesson, T., Treat, C. C., Natali, S. M., Watts, J. D., Potter, S., Lehtonen, A., Mauritz, M., Schuur,

680 E. A. G., Kochendorfer, J., Zona, D., Oechel, W., Kobayashi, H., Humphreys, E., Goeckede, M., Iwata, H., Lafleur, P. M., Euskirchen, E. S., Bokhorst, S., Marushchak, M., Martikainen, P. J., Elberling, B., Voigt, C., Biasi, C., Sonnentag, O., Parmentier, F. W., Ueyama, M., Celis, G., St Louis, V. L., Emmerton, C. A., Peichl, M., Chi, J., Jarveoja, J., Nilsson, M. B., Oberbauer, S. F., Torn, M. S., Park, S. J., Dolman, H., Mammarella, I., Chae, N., Poyatos, R., Lopez-Blanco, E., Christensen, T. R., Kwon, M. J., Sachs, T., Holl, D., and Luoto, M.: Statistical upscaling of ecosystem CO2 fluxes across the terrestrial tundra and boreal domain: Regional patterns and uncertainties, Glob

685 Chang Biol, 10.1111/gcb.15659, 2021.

Wagner, D. N., Shupe, M. D., Persson, O. G., Uttal, T., Frey, M. M., Kirchgaessner, A., Schneebeli, M., Jaggi, M., Macfarlane, A. R., Itkin, P., Arndt, S., Hendricks, S., Krampe, D., Ricker, R., Regnery, J., Kolabutin, N., Shimanshuck, E., Oggier, M., Raphael, I., and Lehning, M.:

Snowfall and snow accumulation processes during the MOSAiC winter and spring season, The Cryosphere Discussions, 10.5194/tc-2021-126, 2021.

690 Wang, W., Rinke, A., Moore, J. C., Ji, D., Cui, X., Peng, S., Lawrence, D. M., McGuire, A. D., Burke, E. J., Chen, X., Decharme, B., Koven, C., MacDougall, A., Saito, K., Zhang, W., Alkama, R., Bohn, T. J., Ciais, P., Delire, C., Gouttevin, I., Hajima, T., Krinner, G., Lettenmaier, D. P., Miller, P. A., Smith, B., Sueyoshi, T., and Sherstiukov, A. B.: Evaluation of air–soil temperature relationships simulated by land surface models during winter across the permafrost region, The Cryosphere, 10, 1721-1737, 10.5194/tc-10-1721-2016, 2016.

Watson, S., Smith, C. D., Lassi, M., and Misfeldt, J.: An Evaluation of the Effectiveness of the Double Alter Wind Shield for Increasing the
695 Catch Efficiency of the Geonor T-200B Precipitation Gauge, Bulletin of the Canadian and Oceanographic Meteorological Society, 36, 168-175, 2008.

Wilcox, E. J., Keim, D., de Jong, T., Walker, B., Sonnentag, O., Sniderhan, A. E., Mann, P., and Marsh, P.: Tundra shrub expansion may amplify permafrost thaw by advancing snowmelt timing, Arctic Science, 5, 202-217, 10.1139/as-2018-0028, 2019.

Williams, M. W., Helmig, D., and Blanken, P.: White on green: under-snow microbial processes and trace gas fluxes through snow, Niwot
700 Ridge, Colorado Front Range, Biogeochemistry, 95, 1-12, 10.1007/s10533-009-9330-z, 2009.

Wilson, G., Green, M., Brown, J., Campbell, J., Groffman, P., Durán, J., and Morse, J.: Snowpack affects soil microclimate throughout the year, Climatic Change, 163, 705-722, 10.1007/s10584-020-02943-8, 2020.

Yi, Y., Kimball, J. S., Chen, R. H., Moghaddam, M., and Miller, C. E.: Sensitivity of active-layer freezing process to snow cover in Arctic Alaska, The Cryosphere, 13, 197-218, 10.5194/tc-13-197-2019, 2019.

705 Yi, Y., Kimball, J. S., Watts, J. D., Natali, S. M., Zona, D., Liu, J., Ueyama, M., Kobayashi, H., Oechel, W., and Miller, C. E.: Investigating the sensitivity of soil respiration to recent snow cover changes in Alaska using a satellite-based permafrost carbon model, Biogeosciences, 17, 5861-5882, 10.5194/bg-2020-182, 2020.

Zermatten, E., Haussener, S., Schneebeli, M., and Steinfeld, A.: Tomography-based determination of permeability and Dupuit–Forchheimer coefficient of characteristic snow samples, 2011.

710 Zhang, T.: Influence of the seasonal snow cover on the ground thermal regime: An overview, Reviews of Geophysics, 43, 10.1029/2004rg000157, 2005.

Zhang, T., Osterkamp, T. E., and Stamnes, K.: Influence of the depth hoar layer of the seasonal snow cover on the ground thermal regime, Water Resources Research, 32, 2075-2086, Doi 10.1029/96wr00996, 1996.
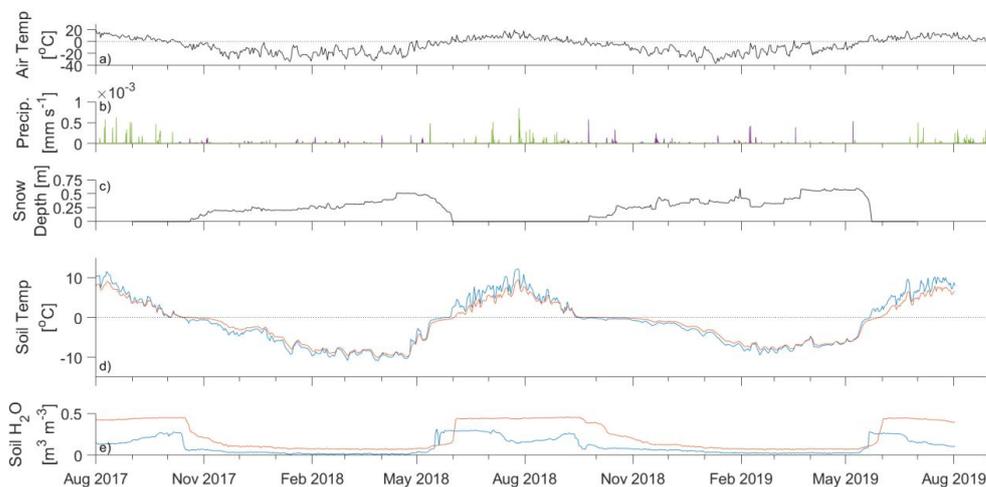
715

Figure 1: Meteorological and soil conditions at Trail Valley Creek from August 2017 to August 2019; a) precipitation: snow (purple) and rain (green), b) snow depth, c) 2 m air temperature, d) soil temperatures at depth of 5 cm (blue) and 20 cm (orange) and e) volumetric soil water content at 5 cm (blue) and 20 cm (orange) depths.

	Snow Depth [cm]	
	March 2018	March 2019
AWS	35	56
Magnaprobe	33 ± 15.7 (n = 14,966)	44 ± 14.4 (n = 8541)
CLM	18	34

720 **Table 1: End of March snow depth summary. Mean and standard deviation of spatially distributed measurements with a sample size greater than n = 1 are shown, otherwise the daily value for 31st March is shown.**
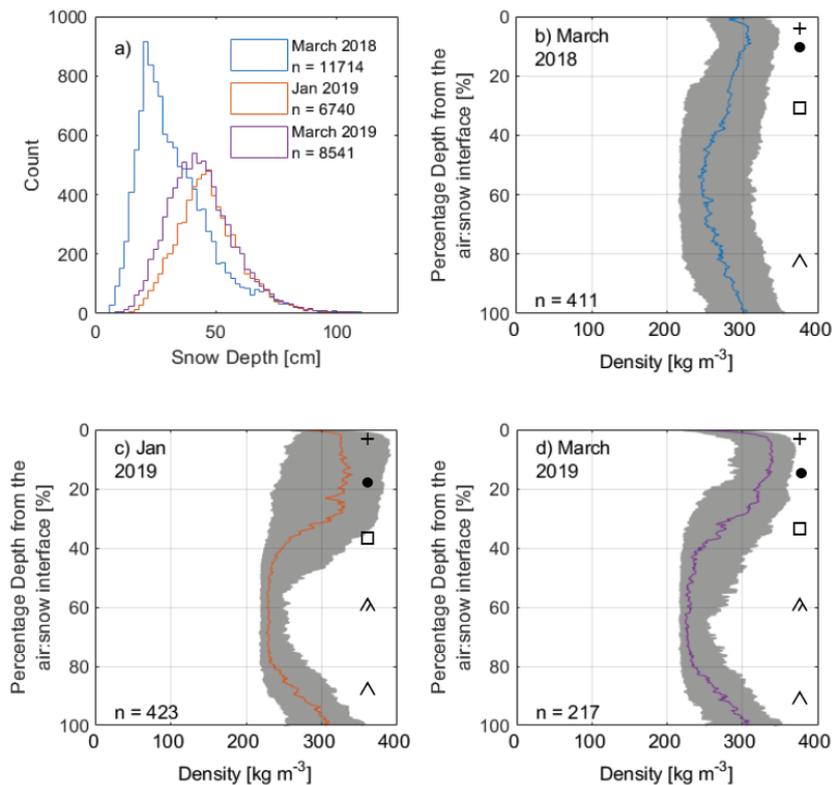
725 **Figure 2: a) Frequency distributions of magnaprobe depths for each sampling campaign where Snow MicroPenetrometer (SMP) measurements are available; b-d) Profiles of median SMP-derived densities (colour-coded for the respective campaigns (Fig. 3a); interquartile range shaded in grey), with snow stratigraphy as per Fierz et al. (2009) superimposed.**

		# of Layers	Layer	Median	Interquartile Range		
Density [kg m^{-3}]	Snowpit Obs.	3	Surface Snow	89	73	152	
			Wind Slab	334	300	365	
			Depth Hoar	249	228	270	
	CLM	4	1	270	209	328	
			2	328	285	346	
			3	340	282	346	
			4	309	291	326	
Thermal Conductivity [W m^{-1} K^{-1}]	Snowpit Obs.	3	Surface Snow	-	-	-	
			Wind Slab	0.20	0.15	0.28	
			Depth Hoar	0.05	0.04	0.06	
	CLM	4	1	0.25	0.17	0.35	
			2	0.35	0.28	0.38	
			3	0.37	0.27	0.38	
			4	0.32	0.29	0.35	

730 **Table 2: Summary of modelled and measured snow densities and thermal conductivities.**
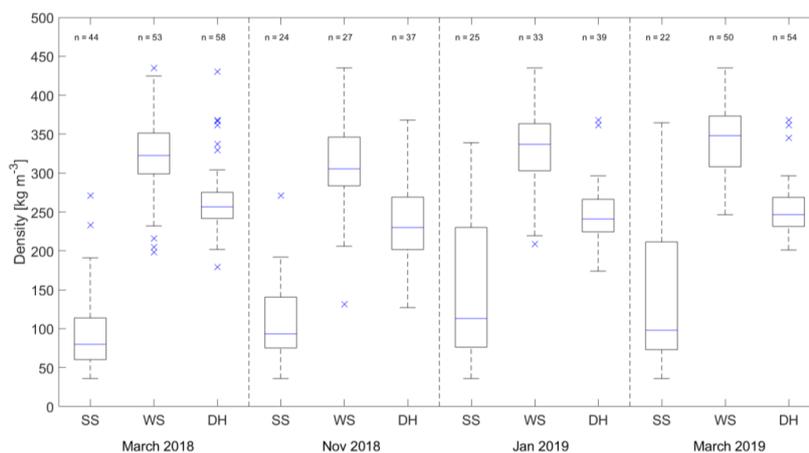
Figure 3: Distributions of measured layer densities (SS = surface snow, WS = wind slab, DH = depth hoar) from four sampling campaigns: box (interquartile range), blue line (median), and whiskers (dashed lines) extend from the end of
735 **each box to 1.5 times the interquartile range; outliers beyond this range (blue crosses).**
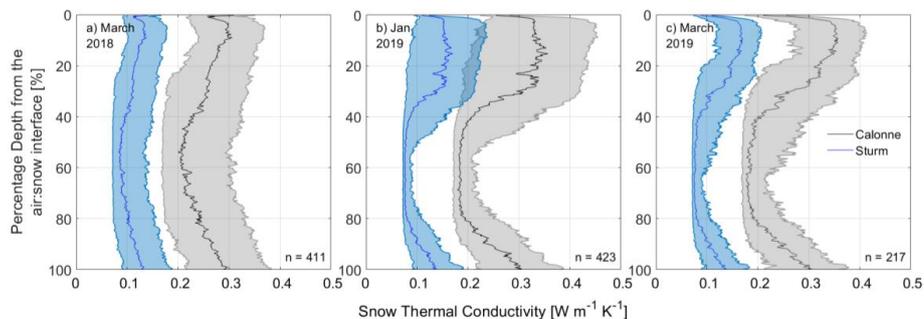
Figure 4: Median thermal conductivity profiles (lines) and interquartile range (shaded areas) approximated from SMP densities, using the parameterisations of Calonne et al. (2011) in black, and Sturm et al. (1997) in blue.

740
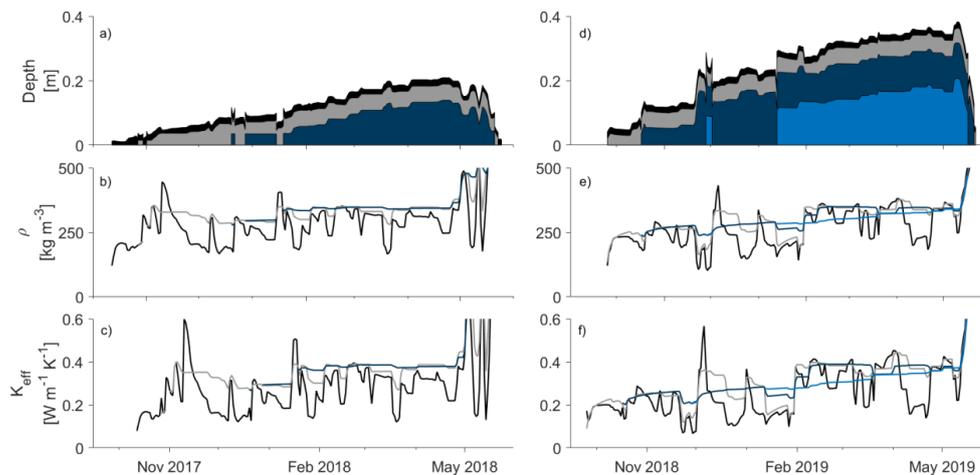
745   **Figure 5: Simulated snow layers and their properties for winter 2017-18; a) simulated snow layer thicknesses, b) snow layer densities, c) snow layer thermal conductivities; d) to f) as before but for winter 2018-19.**
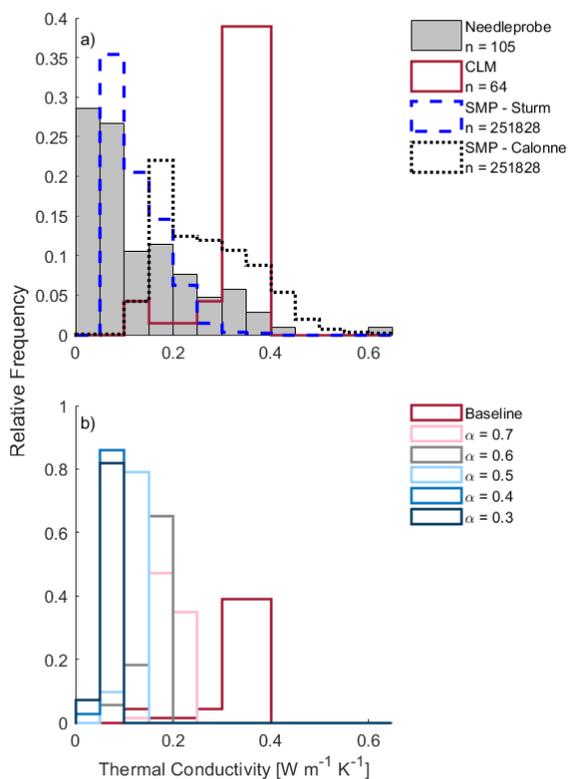
Figure 6: a) Histograms of measured and simulated thermal conductivity from March 2018 and 2019 sampling campaigns, b) Sensitivity testing of simulated thermal conductivities for the same time period. Note the different scales on the y-axes.
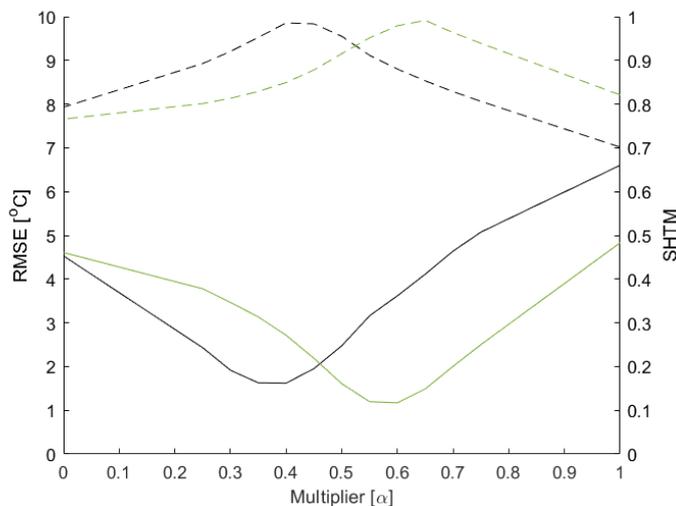
Figure 7: Changes to model performance when adjusting snow thermal conductivity, measured using RMSE of 10cm soil temperatures (solid lines) and the Snow Heat Transfer Metric (SHTM – dashed lines) for the 2017-18 (black) and 2018-19 (green) snow seasons.
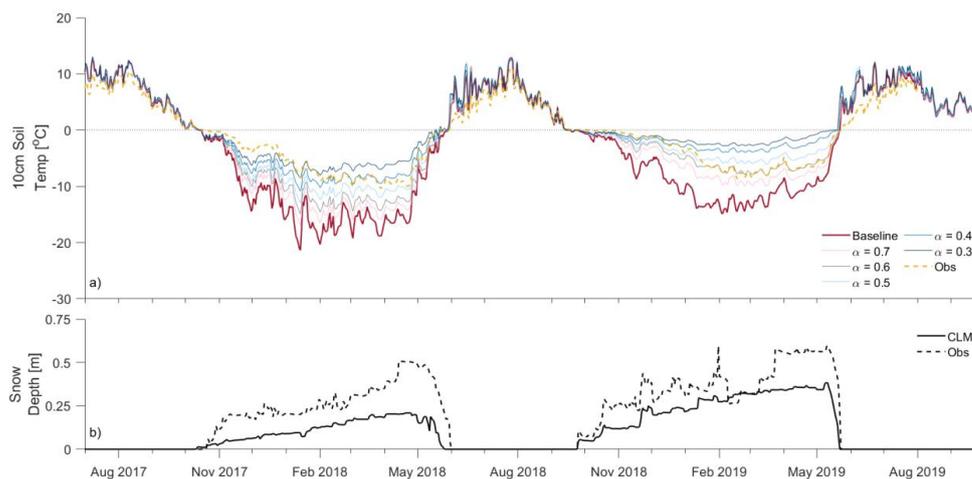
Figure 8: a) Timeseries of 10cm soil temperatures timeseries for K_{eff} sensitivity tests compared to field measurements, b) Observed and simulated snow depths for the same time period.
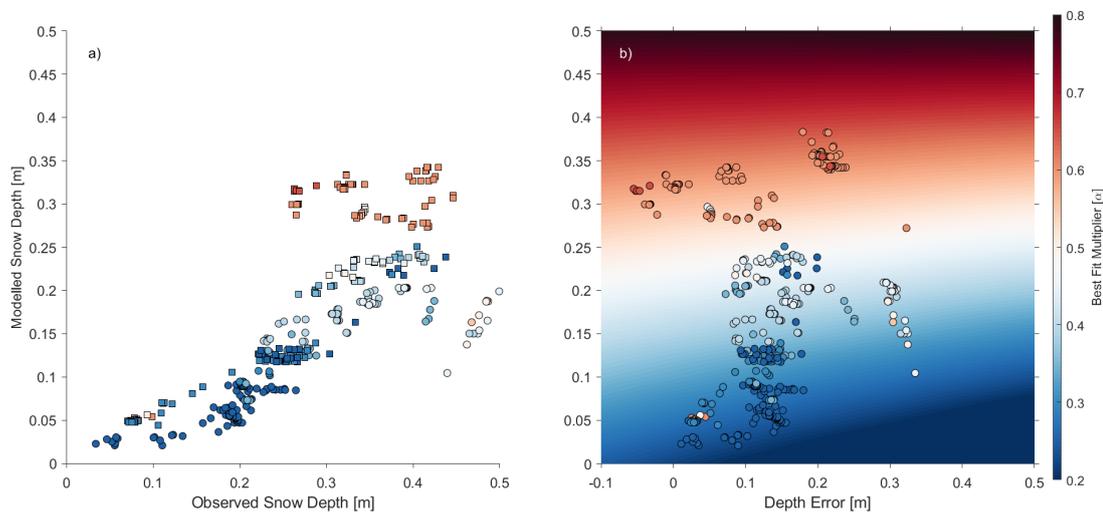
Figure 9: Influence of observed (x-axis; a) and modelled (y-axis; both) snow depth and snow depth error (x-axis; b) on the best fit correction (colour) at each timestep for both the 2017-18 (circles) and 2018-19 (squares) snow seasons.
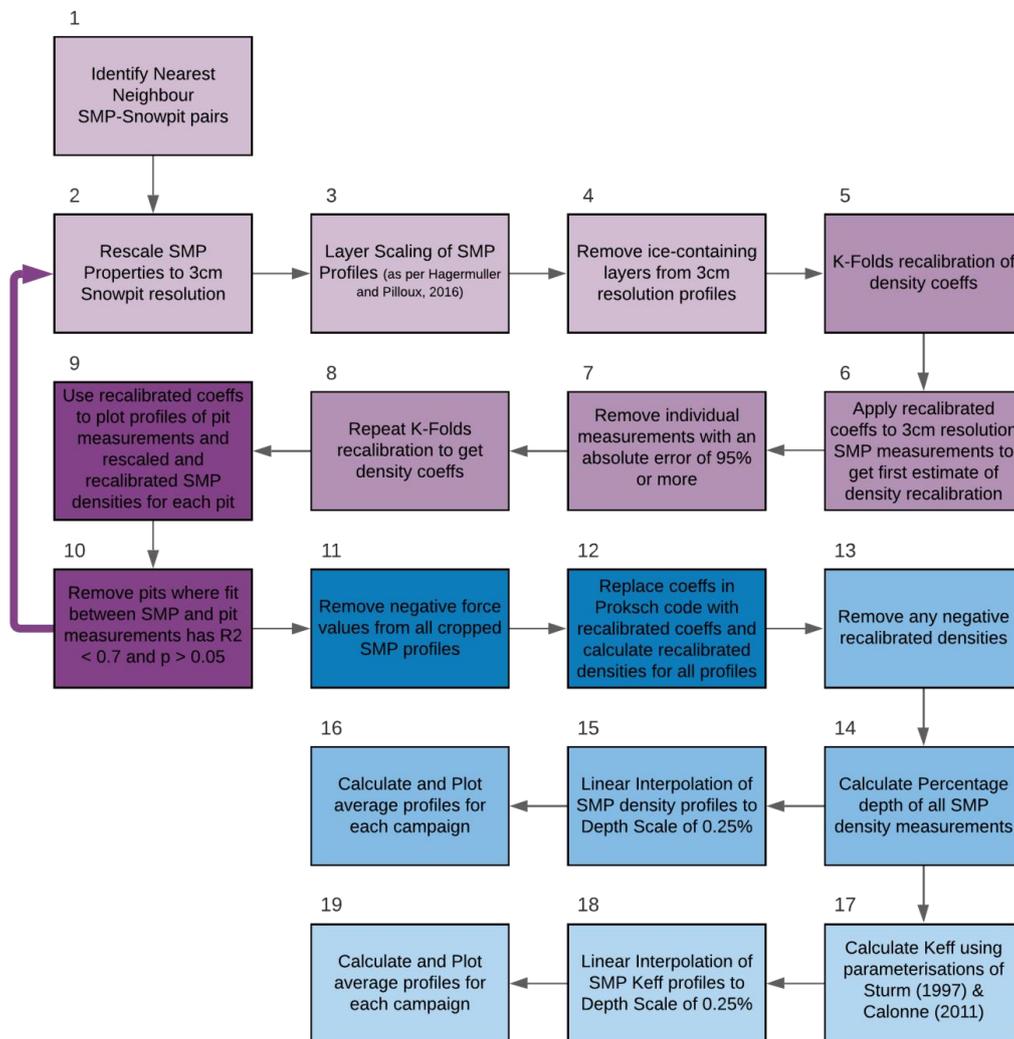
Figure A1: Recalibration process for SMP densities. Steps 2-9 (purple) mirror the process of King et al. (2020b), with
765 **Step 10 providing a quantitative threshold to assess whether the recalibration attempt is successful. Steps 11 to 19 (blue)**
apply the recalibration to the TVC dataset and derive thermal conductivity profiles from the recalibrated SMP
densities.

	a	*b*	*c*	*d*
Proksch (2015)	420.47	102.47	-121.15	-169.96
King (2020b)	312.54	50.27	-50.26	-88.15
This Study	***307.36***	***43.51***	***-38.95***	***-79.36***

Table A1: Coefficients used to calculate density from SMP measurements.
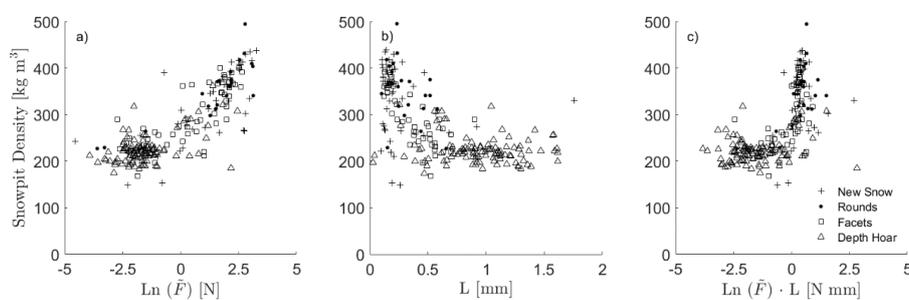
Figure A2: Relationships between the snowpit densities and SMP microstructural metrics from the paired profiles in the recalibration dataset, after Figure 5 of King et al. (2020b).
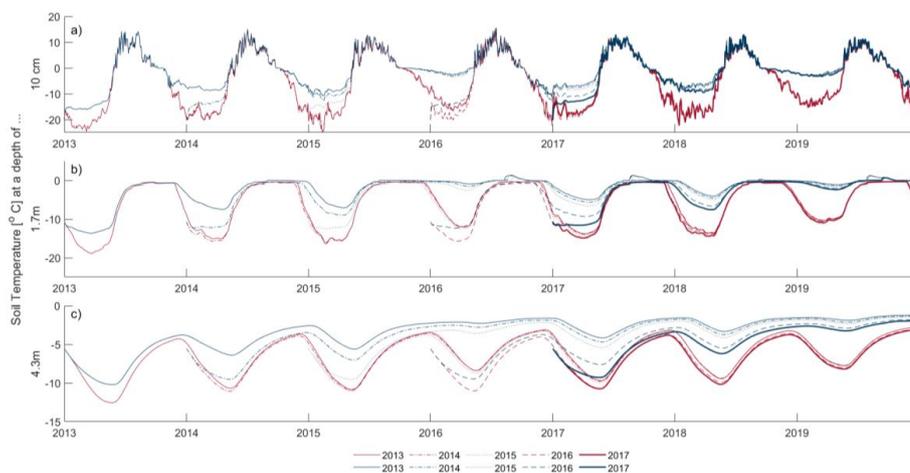
Figure B1: Soil temperatures at a) 10 cm, b) 1.7 m and c) 4.3 m (third, eleventh and sixteenth CLM soil layers) for varying lengths of model spin-up (line styles; all spin-ups from 1 January, year given in legend), for both baseline (α = 1; dark red) and K_{eff} adjusted (α = 0.3; navy blue) model conditions.